

# Numerical Research on Energy Evolution and Burst Behavior of Unloading Coal–Rock Composite Structures

Yan-chun Yin  · Yun-liang Tan · Yan-wei Lu · Yu-bao Zhang

Received: 28 February 2018 / Accepted: 12 June 2018 / Published online: 14 June 2018  
© Springer International Publishing AG, part of Springer Nature 2018

**Abstract** In order to research the evolution of energy stored in the composite coal-rock structure and coal fragments' burst characteristics, lateral pressure unloading numerical tests of composite coal–rock models with different Young's modulus were carried by PFC2D software. The research showed that the accumulated strain energy and kinetic energy in the coal was greater than that in roof and floor, and particles in the coal had a longer burst distance. The variation of the kinetic energy in the model could be separated into initialized burst, rapid burst, stable burst and residual burst stage. With the increase of the coal's Young's modulus, the accumulated amount and releasing velocity of strain energy in the coal decreased in the form of a power function, while the strain energy in both roof and floor changed little. The maximum value of the kinetic energy in the coal was negative linearly related to the Young's modulus of the coal, while that of the rock was positive

linearly. When the Young's modulus of the coal was increased, particles bursted with a shorter distance, and most particles accumulated near the coal wall.

**Keywords** Underground mining · Rockburst · Coal–rock composite body · Burst energy · Particle flow simulation

## 1 Introduction

Rockburst is a typical disaster caused by underground excavation (Dou et al. 2014; Kouame et al. 2017; Manouchehrian and Cai 2016b; Stacey 2016). Rockburst gestation process is completed, and the entire burst process is hard to be recorded. Many kinds of methods are utilized to reveal the mechanism of the rock burst (Guo et al. 2017; Song et al. 2017; Wang et al. 2017c), including laboratory tests (Tajdus et al. 2014), in situ monitoring (Morissette et al. 2017; Tan et al. 2015, 2017; Wang et al. 2017a; Zhao et al. 2017, 2018) and simulation methods (Adoko et al. 2013; Cai et al. 2016; Manouchehrian and Cai 2016a; Zhang et al. 2018; Zhao et al. 2014). Rock burst mechanism is revealed at two main aspects, stress and energy. At the aspect of stress, some scholars think that rock burst is caused by excavation unloading process or stress concentration (Liu et al. 2017). He et al. (2014, 2015) carried out the granite rockburst

---

Y. Yin (✉) · Y. Tan · Y. Lu · Y. Zhang  
State Key Laboratory of Mining Disaster Prevention and Control Co-founded by Shandong Province and the Ministry of Science and Technology, Shandong University of Science and Technology, Qingdao 266590, Shandong, China  
e-mail: yycrsd@163.com

Y. Yin · Y. Tan · Y. Lu · Y. Zhang  
College of Mining and Safety Engineering, Shandong University of Science and Technology, Qingdao 266590, Shandong, China

tests under four different unloading rates by using the self-developed testing system for rockburst, and the testing results indicated that the number and portion of fragments with blocky structure decreased with the unloading rate dropping down. At the aspect of energy, some scholars think that rockburst is caused by a sudden release of the elastic strain energy stored in the rock (Feng et al. 2016; Lindin and Lobanova 2013), and accumulation and releasing law of the energy was studied (Wang et al. 2017b; Wu et al. 2016; Xue et al. 2016). Ning et al. (2018) found that the variation in the pre-peak energy-dissipation ratio was consistent with the coal damage, and proposed a new energy-dissipation method to identify crack initiation and propagation thresholds, which was a potential tool for early warning of rockburst.

In the mining engineering, rockburst is a dynamic phenomenon of the sudden failure of the roof-coal-floor structure. The interaction between rock and coal plays an important role in keep equilibrium of the roadway and working face. In recent years, mechanical properties of composite coal–rock structure have been studied, and some outstanding achievements have been obtained. Zhao et al. (2016) researched the influence of the interfacial angle on failure characteristics of composite coal–rock mass, and proposed four typical failure patterns. Zuo et al. (2013) found that the confining pressure and loading conditions influence composite coal–rock mass' failure mode obviously.

In previous study, the tests of the composite coal–rock samples were under loading conditions generally (Lu et al. 2007). But in the roadway excavation of mining engineering, the coal and rock at the heading face are in unloading process (Huang et al. 2018). When excavating in a high stress concentration area with a large footage, the high stress can not transferred into the deeper rocks immediately, and the coal and rock in the plastic zone can burst out easily, as shown in Fig. 1. The mechanical behavior and energy evolution law at this engineering condition was less studied. In this paper, a composite coal–rock model was established using PFC2D, and the lateral pressure unloading tests were carried out. The energy releasing and particles' burst law with different Young's modulus of the coal were studied.

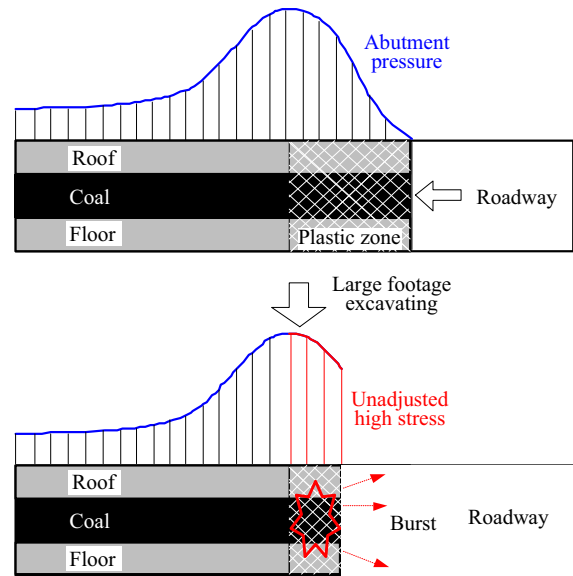


**Fig. 1** Excavating process of the roadway

## 2 Testing Theories and Methods

### 2.1 Rationale of Particle Flow Code

Particle flow code in two dimensions (PFC2D) is a software used to simulate discrete elements. As an effective approach for researching geotechnical mechanics, it reflects the macroscopic mechanical behaviour of materials using microscopic changes by analysing the motion and interaction of micro-particles. In PFC2D, bond models are generally used for studying geotechnical materials. They include contact bond and parallel bond models. The former expresses the bond at points between particles, and is generally used to simulate granular materials such as soil, while the latter expresses the bonding of surfaces between particles, and is always used to simulate compact materials, such as rocks (Haeri and Sarfarazi 2016; Haeri et al. 2017; Yin et al. 2015).

In parallel bond model, eight parameters should be defined: friction coefficient, normal and shear contact stiffness  $k_n$  and  $k_s$ , normal and shear parallel stiffness  $\bar{k}_n$  and  $\bar{k}_s$ , normal and shear bonding strength  $\sigma_n$  and  $\sigma_s$ , and bond radius  $\lambda$ . The parameters can be calculated by Eq. (1) (Potyondy and Cundall 2004).

$$\begin{cases} k_n = 2E_c \\ k_s = \frac{k_n}{k_n/k_s} \\ \bar{k}_n = \frac{\bar{E}_c}{2\bar{r}} \\ \bar{k}_s = \frac{\bar{k}_n}{k_n/k_s} \end{cases} \quad (1)$$

where  $E_c$  and  $\bar{E}_c$  is the Young’s modulus of the contact and parallel bond;  $\bar{r}$  is the mean radius of the contact particles. Young’s modulus  $E_c$  and  $\bar{E}_c$  are often set to be the same value.  $\sigma_n$  and  $\sigma_s$  can be set as the compressive strength.  $\lambda$  is set to be 1 generally.

### 2.2 Burst Modelling

A composite coal–rock model established in PFC2D is shown in Fig. 2. Being 4 m in height and 1 m in width, this model consists of roof, coal, and floor, with the height of 1, 2, and 1 m, respectively. Table 1 lists the micro-parameters of each strata. During the test, the stress applied on the model was loaded to 40 MPa firstly, to simulate the high stress to make the model into plastic state. And then the stress was unloaded to 30 MPa as the average value of the high stress. The lateral restraint on the right side of the model was removed. As a result, the particles in this model bursted towards the roadway. Meanwhile, the internal strain energy, kinetic energy of the particles, and burst displacement in the model were monitored.

### 2.3 Burst Energy Calculating Approach

In particle flow code, the strain energy  $E_s$  accumulated in the model includes two parts: contact strain energy  $E_s^c$  and parallel strain energy  $E_s^{pb}$  (Itasca Consulting

Group 2008). The strain energy can be calculated by Eqs. (2)–(4).

$$E_s = E_s^c + E_s^{pb} \quad (2)$$

$$E_s^{pb} = \frac{1}{2} \sum_{i \in N_{pb}} \left( \frac{|\bar{F}_i^n|^2}{A_i \bar{k}_i^n} + \frac{|\bar{F}_i^s|^2}{A_i \bar{k}_i^s} + \frac{|\bar{M}_i|^2}{I_i \bar{k}_i^n} \right) \quad (3)$$

$$E_s^c = \frac{1}{2} \sum_{i \in N_c} \left( \frac{|F_i^n|^2}{k_i^n} + \frac{|F_i^s|^2}{k_i^s} \right) \quad (4)$$

where  $\bar{F}_i^n$ ,  $\bar{F}_i^s$ ,  $\bar{M}_i$  is the normal force, shear force and the moment in the parallel bond  $i$ ;  $F_i^n$  and  $F_i^s$  is the normal force and shear force in the contact  $i$ ;  $A_i$  and  $I_i$  is the area and inertia moment of the bond cross section;  $N_c$ ,  $N_{pb}$  is the number of contacts and parallel bonds.

The kinetic energy  $E_k$  is accounted for both translational and rotational motion, and can be expressed by Eq. (5).

$$E_k = \frac{1}{2} \sum_{i \in N_p} \left( mv_x^2 + mv_y^2 + Iw^2 \right) \quad (5)$$

where  $N_p$  is the number of particles;  $m$  is the mass of the particle;  $v_x$  and  $v_y$  is the  $x$ -component and  $y$ -component of the particle’s velocity;  $w$  is the rotational velocity.

## 3 Results and Discussion

### 3.1 Release of Energy During Burst

Under the influence of external load, strain energy was accumulated in the composite coal–rock model. When the lateral restraint was removed, the composite coal–rock model rapidly lost its stability and was therefore fractured. Accordingly, the strain energy accumulated in the model was released rapidly. Figure 3 shows the curves of strain energy releasing for different Young’s modulus of the coal.

By analyzing the curves in Fig. 3, it was found that:

1. For the composite coal–rock model, the strain energy accumulated in the coal was great, while that in roof and floor was low. The release of strain energy in the total model and the coal was divided into two stages: the first stage was a linear release stage, during which the energy was rapidly

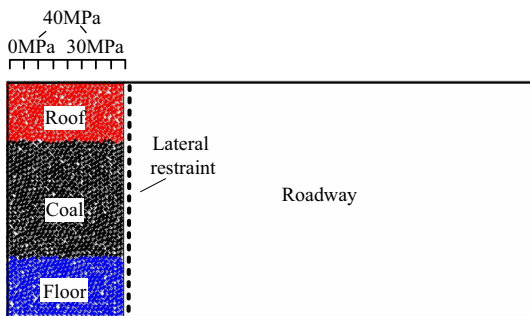
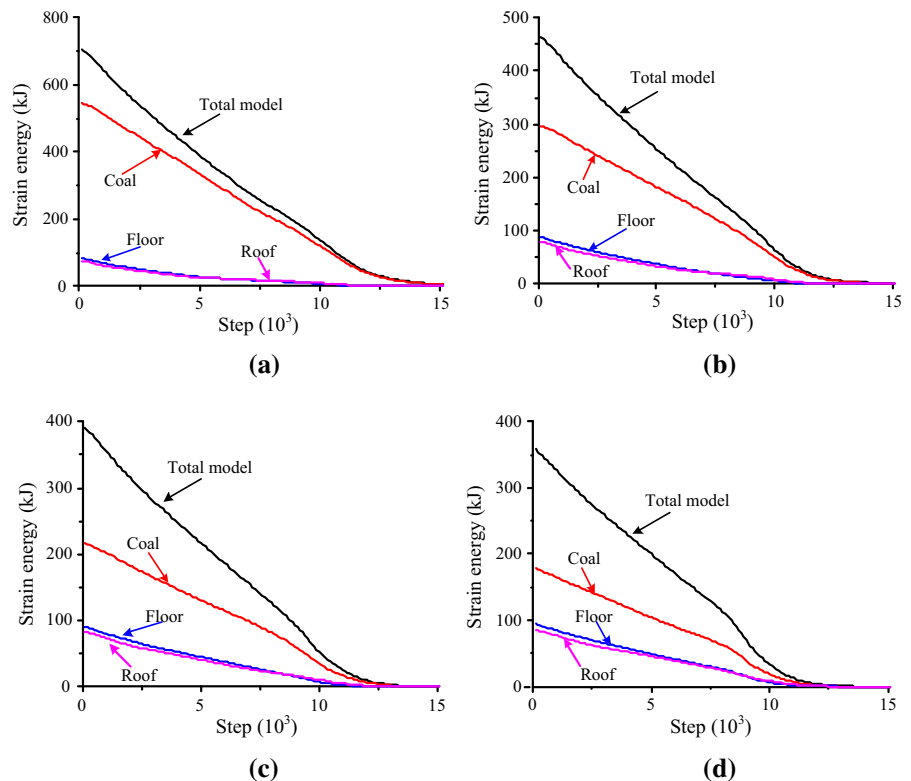


Fig. 2 The composite coal–rock particle flow model

**Table 1** Parameters of the composite coal–rock model

Structure	Density ( $\text{kg/m}^3$ )	Radius (mm)	Friction coefficient	Bond radius	Young's modulus (GPa)	Bonding strength (MPa)
Roof	2400	4	0.5	1	5	30
Coal	1400	4	0.5	1	0.5, 1, 1.5, 2	10
Floor	2400	4	0.5	1	5	30
Interface	–	–	0.5	1	0.5	10

**Fig. 3** Strain energy releasing curves for coal's Young's modulus be **a** 0.5 GPa, **b** 1 GPa, **c** 1.5 GPa, and **d** 2 GPa

released at an approximately constant speed; while during the second stage, energy was released at a rate best modelled by a power function. That is, the releasing rate of strain energy gradually decreased. In contrast, the strain energy in the roof and floor was slowly released at an approximately linear rate. Moreover, energy was released completely from these strata before its release from the coal.

- When the Young's modulus of the coal was changed, the strain energy accumulated in the model changed accordingly, as shown in Table 2 and Fig. 4. According to the Eq. (2)–(4) used for

calculating strain energy, it was found that strain energy was inversely proportional to the stiffness of the particle. When the Young's modulus of the coal was increased, the stiffness of the particles therein increased, while the strain energy accumulated in the coal decreased under the same external load. In contrast, since the modulus of both roof and floor remained the same, the amount of strain energy stored therein was changed little. With the increase of the Young's modulus of the coal, the decreasing gradient of strain energy in the total model and the coal was gradually reduced, and on the whole, the maximum

**Table 2** Released strain energy for different Young’s modulus of the coal

Young’s modulus (GPa)	Maximum strain energy (kJ)				Energy releasing velocity (J/step)			
	Total model	Coal	Floor	Roof	Total model	Coal	Floor	Roof
0.5	704.18	545.33	83.06	75.79	60.39	43.70	8.91	7.78
1	464.06	296.67	87.94	79.45	40.89	23.60	9.26	8.03
1.5	389.91	216.06	90.89	82.96	33.63	16.99	8.71	7.93
2	358.01	178.03	94.41	85.57	30.96	14.52	8.70	7.74

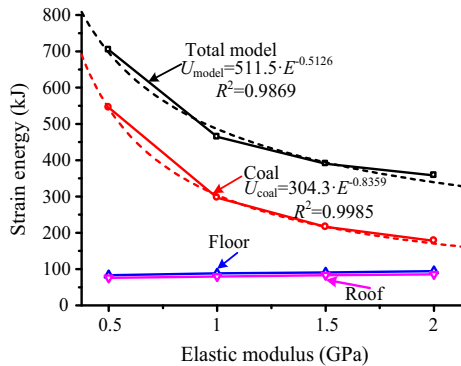


**Fig. 4** Relationship between the maximum strain energy and the Young’s modulus of the coal

accumulated amount of strain energy and the Young’s modulus of the coal presented a power function relationship.

- When the Young’s modulus of the coal was increased, the releasing velocity of strain energy reduced correspondingly, as shown in Table 2 and Fig. 5. The releasing velocity of strain energy in the total model and the coal was related to the Young’s modulus of the coal by a power function,

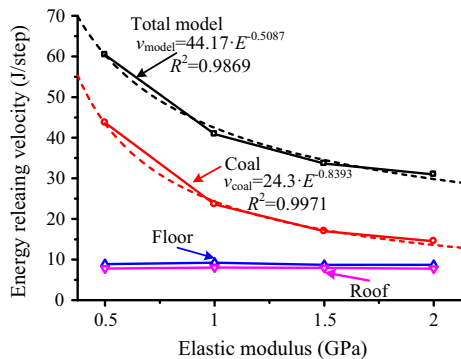


**Fig. 5** Relationship between the releasing velocity of strain energy and the Young’s modulus of the coal

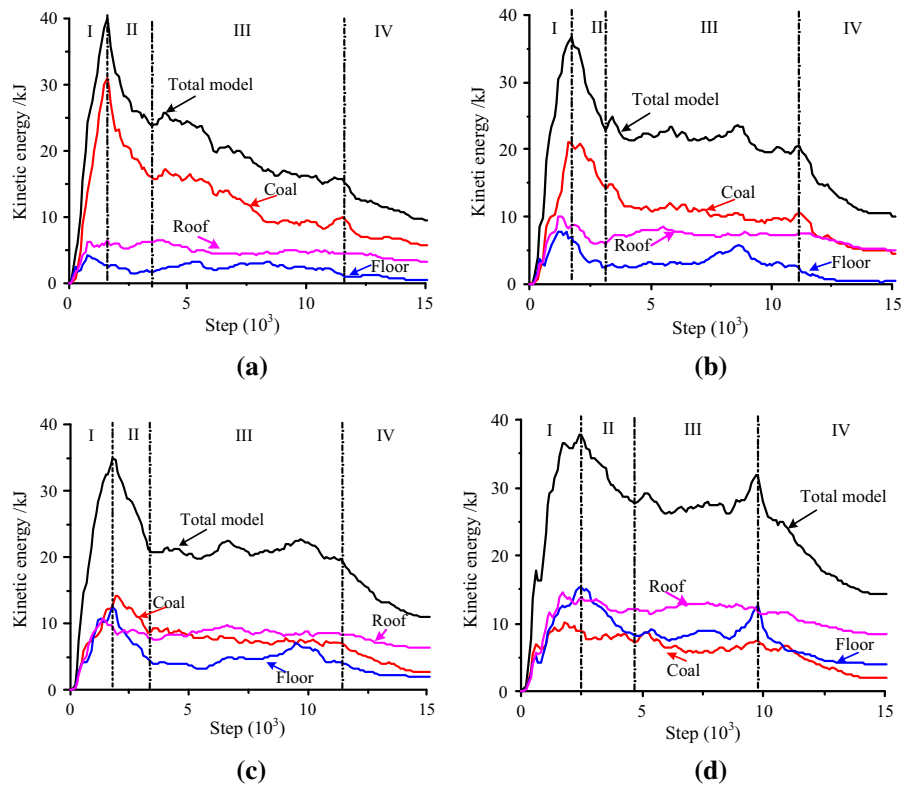
while the releasing velocity of energy in both roof and floor changed little.

### 3.2 Kinetic Energy Variation

The strain energy accumulated in the composite coal–rock model was generally released as kinetic energy and frictional energy. Thereinto, the kinetic energy contributed significantly to the burst damage. When the lateral restraint on the model was removed, the strain energy therein was released. Meanwhile, the particles in the model were ejected with a certain kinetic energy. The variation of kinetic energy in the coal for different elastic modulus is shown in Fig. 6. It can be seen from Fig. 6 that:

- After the strain energy of the model was released, the variation of the kinetic energy in the model could be separated into four stages: the first one was an initialisation of the burst phase. Particles on the surface of the model accelerated to an extremely high burst velocity in a short time, and kinetic energy of the model increased rapidly to its peak value. The second stage was a rapid burst stage. After particles had accelerated to such extremely high velocities, they moved outwards rapidly and therefore the energy was released quickly. Thirdly, a stable burst stage developed, during which the kinetic energy of some particles ejected from the model decreased due to a lack of energy at the rock burst source. As a consequence, the particles inside began to be subjected to a certain kinetic energy and the total kinetic energy of the model became stable. The final stage was a residual burst phase, and all the strain energy in the model had been released so that the kinetic energy of the model decreased rapidly to zero.

**Fig. 6** Curves of kinetic energy variation for coal's Young's modulus be **a** 0.5 GPa, **b** 1 GPa, **c** 1.5 GPa, and **d** 2 GPa



2. When the Young's modulus of the coal increased, the strain energy in the coal was decreased, which decreased the available power driving subsequent particle motion. As a result, the kinetic energy imparted to the particles gradually decreased (see Fig. 7). More strain energy was transferred to the roof and floor and then released, thus increasing their kinetic energy. The maximum value of the kinetic energy of the coal was negative linearly

related to the Young's modulus of the coal, while that of the rock was positive linearly. When the Young's modulus of the coal was 0.5 or 1 GPa (approximately 20–40% of that of the rock) the kinetic energy of the coal was larger than that of the rock; when the Young's modulus of the coal was 1.5 GPa (i.e. 60% of that of the rock), little difference was found between the kinetic energy of the coal and the rock; while for 2 GPa (i.e. 80% of that of the rock), the kinetic energy of the rock exceeded that of the coal. In general, the peak value of the kinetic energy of the rock was linearly related to the Young's modulus of the coal. The total kinetic energy of the total model first decreased, and then increased, with no clear pattern in this behaviour.

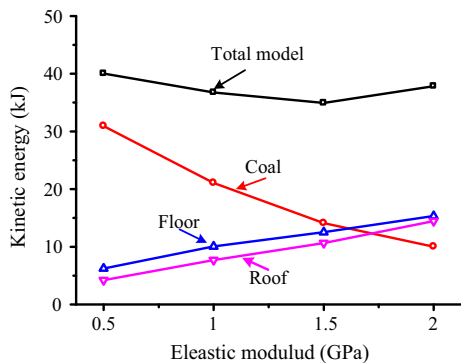


**Fig. 7** Relationship between the maximum kinetic energy and the Young's modulus of the coal

### 3.3 Burst Process of Particles

After the strain energy in the composite coal–rock model was released, particles instantly lost their stability and were ejected. The burst process of particles is shown in Fig. 8. When the strain energy

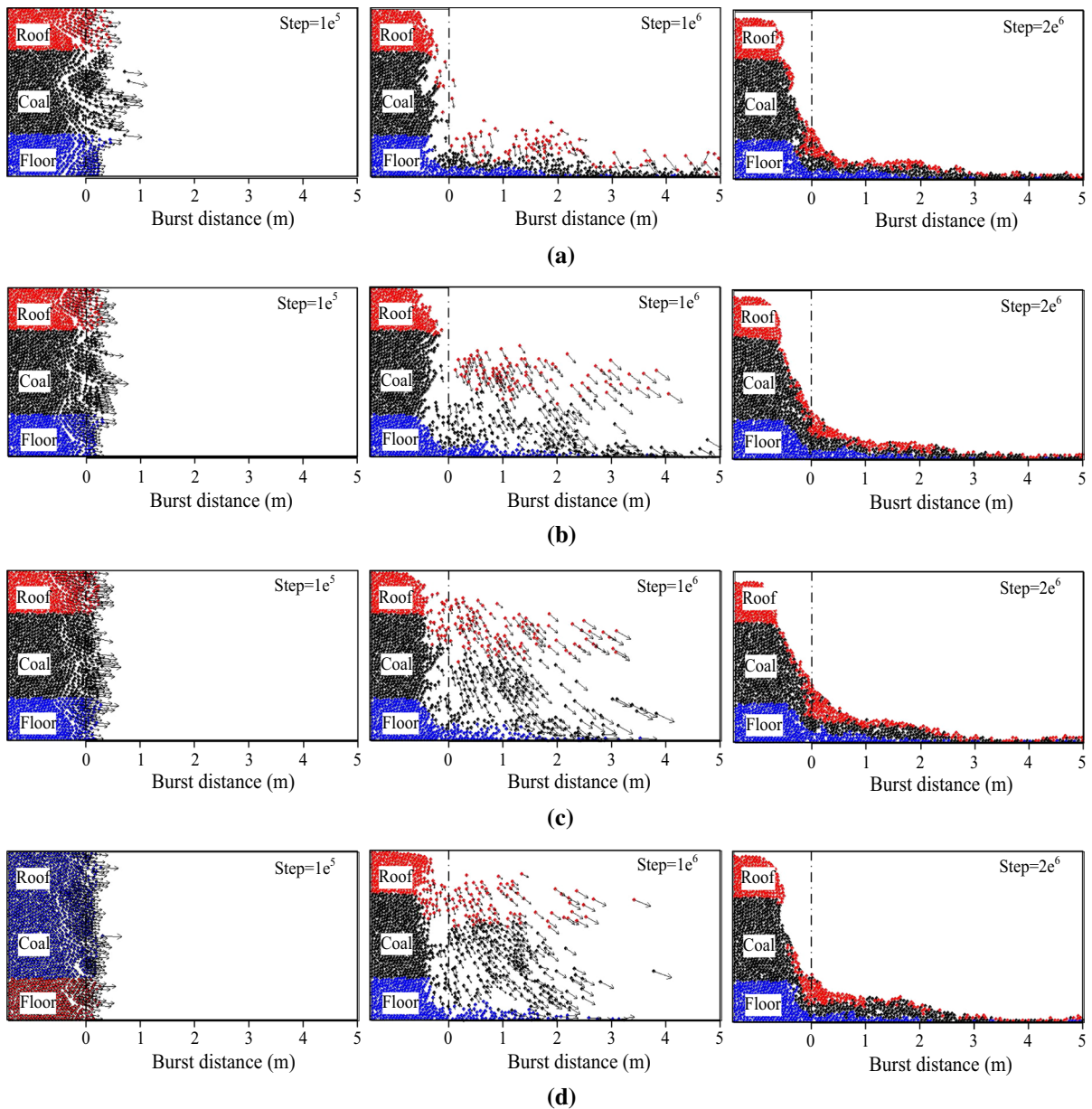


**Fig. 8** Burst process of particles for coal's Young's modulus be **a** 0.5 GPa, **b** 1 GPa, **c** 1.5 GPa, and **d** 2 GPa

was released, the particles on the surface of the model first reached a high burst velocity and rushed out the greatest distances. Particles inside the model got a lower burst velocity following closely, for the releasing of strain energy. So these particles had shorter burst distances. The number of particles decreased with the increasing distance from the coal wall. The higher the accumulated amount of strain energy and kinetic energy, the further each particle travelled.

When the Young's modulus of the coal increased, the strain energy in the model was decreased, and particles were ejected shorter distances. So most particles began to accumulate near the coal wall. Therefore, the number of particles far from the coal wall decreased, as shown in Fig. 9.

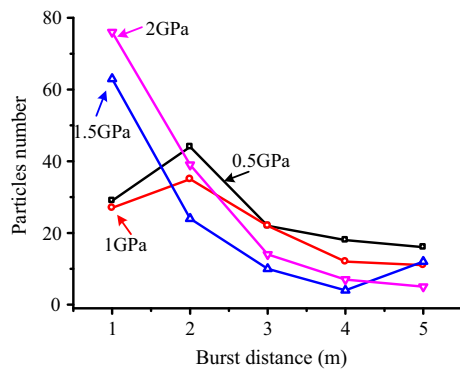


**Fig. 9** Burst distances of coal with different Young's modulus

### 3.4 Discussion

In the composite coal–rock model, when the coal breaks, the strain energy accumulated in the rock releases. Under high stress, the released energy of the rock transforms into kinetic energy and external power on the coal. When the difference between the coal's and rock's Young's modulus is high, more released energy is applied on the coal, and the coal bursts out fast. Therefore, when mining in “hard–soft–hard” coal seams under high stress, the mining speed should be slow down to ensure the peak value of abutment pressure transfers into deep coal by stress adjustment.

## 4 Conclusions

Based on the lateral pressure unloading numerical tests of composite coal–rock models at different Young's modulus, the energy releasing and particles' burst characteristics were studied, and the following conclusions are drawn:

1. The strain energy accumulated in the coal was greater than that in roof and floor. With the increase of Young's modulus of the coal, the amount and releasing velocity of strain energy in the coal decreased in the form of a power function, while the strain energy in both roof and floor changed little.
2. The variation of the kinetic energy in the model could be separated into initialized burst, rapid burst, stable burst and residual burst stage. The maximum value of the kinetic energy of the coal was negative linearly related to the Young's

modulus of the coal, while that of the rock was positive linearly.

3. With higher strain energy and kinetic energy, particles in the coal had longer burst distances. When the Young's modulus of the coal increased, particles' burst distances decreased, and most particles began to accumulate near the coal wall.

**Acknowledgements** This research described in this paper was financially supported by National Natural Science Foundation of China (51604165, 51474137, 11602130), Tai'shan Scholar Engineering Construction Fund of Shandong Province of China (ts201511026), and Scientific Research Foundation of Shandong University of Science and Technology for Recruited Talents (2016RCJJ027).

## References

- Adoko AC, Gokceoglu C, Wu L et al (2013) Knowledge-based and data-driven fuzzy modeling for rockburst prediction. *Int J Rock Mech Min Sci* 61:86–95
- Cai W, Dou LM, Si GY et al (2016) A principal component analysis/fuzzy compressive evaluation model for coal burst liability assessment. *Int J Rock Mech Min Sci* 81:62–69
- Dou LM, Cai W, Song SY et al (2014) Dynamic risk assessment of rock burst based on the technology of seismic computed tomography detection. *J China Coal Soc* 39(2):238–244 (**In Chinese**)
- Feng JJ, Wang EY, Shen RX et al (2016) Investigation on energy dissipation and its mechanism of coal under dynamic loads. *Geomech Eng* 11(5):657–670
- Guo WY, Zhao TB, Tan YL et al (2017) Progressive mitigation method of rock bursts under complicated geological conditions. *Int J Rock Mech Min Sci* 96:11–22
- Haeri H, Sarfarazi V (2016) Numerical simulation of tensile failure of concrete using particle flow code (PFC). *Comput Concrete* 18(1):39–51
- Haeri H, Sarfarazi V, Zhu ZM (2017) Effect of normal load on the crack propagation from pre-existing joints using particle flow code (PFC). *Comput Concrete* 19(1):99–110
- He MC, Zhao F, Du S et al (2014) Rockburst characteristics based on experimental tests under different unloading rates. *Rock Soil Mech* 35(10):2737–2748 (**In Chinese**)
- He MC, Souas LRE, Miranda T et al (2015) Rockburst laboratory tests database—application of data mining techniques. *Eng Geol* 185:116–130
- Huang WP, Yuan Q, Tan YL et al (2018) An innovative support technology employing a concrete-filled steel tubular structure for a 1000-m-deep roadway in a high in situ stress field. *Tunn Undergr Space Technol* 73:26–36
- Itasca Consulting Group I (2008) Theory and background: energy tracing. Particle flow code in 2 dimensions
- Kouame KJA, Jiang FX, Zhu ST (2017) Research on cause of dynamic disaster of deep mining control in China and its further prevention application in Ivory Coast. *Geotech Geol Eng* 35(3):1141–1149



- Lindin GL, Lobanova TV (2013) Energy sources of rockbursts. *J Min Sci* 49(1):36–43
- Liu ZG, Cao AY, Zhu GA et al (2017) Numerical simulation and engineering practice for optimal parameters of deep-hole blasting in sidewalls of roadway. *Arab J Sci Eng* 42(9):3809–3818
- Lu CP, Dou LM, Wu XR (2007) Experimental research on rules of rockburst tendency evolution and acoustic-electromagnetic effects of compound coal–rock samples. *Chin J Rock Mech Eng* 26(12):2549–2555 (**In Chinese**)
- Manouchehrian A, Cai M (2016a) Influence of material heterogeneity on failure intensity in unstable rock failure. *Comput Geotech* 71:237–246
- Manouchehrian A, Cai M (2016b) Simulation of unstable rock failure under unloading conditions. *Can Geotech J* 53(1):22–34
- Morissette P, Hadjigeorgiou J, Punkkinen AR et al (2017) The influence of mining sequence and ground support practice on the frequency and severity of rockbursts in seismically active mines of the Sudbury Basin. *J S Afr Inst Min Metall* 117(1):47–56
- Ning JG, Wang J, Jiang JQ et al (2018) Estimation of crack initiation and propagation thresholds of confined brittle coal specimens based on energy dissipation theory. *Rock Mech Rock Eng* 51(1):119–134
- Potyondy DO, Cundall PA (2004) A bonded-particle model for rock. *Int J Rock Mech Min Sci* 41:1329–1364
- Song DZ, Wang EY, Li ZH et al (2017) EMR: an effective method for monitoring and warning of rock burst hazard. *Geomech Eng* 12(1):53–69
- Stacey TR (2016) Addressing the consequences of dynamic rock failure in underground excavations. *Rock Mech Rock Eng* 49(10):4091–4101
- Tajdus A, Cieslik J, Tajdus K (2014) Rockburst hazard assessment in bedded rock mass: laboratory tests of rock samples and numerical calculations. *Arch Min Sci* 59(3):591–608
- Tan YL, Yu FH, Ning JG et al (2015) Design and construction of entry retaining wall along a gob side under hard roof stratum. *Int J Rock Mech Min Sci* 77:115–121
- Tan YL, Liu XS, Ning JG et al (2017) In situ investigations on failure evolution of overlying strata induced by mining multiple coal seam. *Geotech Test J* 40(2):244–257
- Wang HW, Jiang YD, Xue S et al (2017a) Investigation of intrinsic and external factors contribution to the occurrence of coal bumps in the Mining Area of Western Beijing, China. *Rock Mech Rock Eng* 50(4):1033–1047
- Wang J, Ning JG, Jiang JQ et al (2017b) Research on the energy criterion for rockbursts induced by broken hard and thick rock strata and its application. *Geotech Geol Eng* 35(2):731–746
- Wang SR, Li CY, Yan WF et al (2017c) Multiple indicators prediction method of rock burst based on microseismic monitoring technology. *Arab J Geosci*. <https://doi.org/10.1007/s12517-017-2946-8>
- Wu D, Liu YC, Zheng ZX et al (2016) Impact energy absorption behaviour of cemented coal gangue-fly ash backfill. *Geotech Geol Eng* 34(2):471–480
- Xue Y, Gao F, Teng T et al (2016) Effect of gas pressure on rock burst proneness indexes and energy dissipation of coal samples. *Geotech Geol Eng* 34(6):1737–1748
- Yin YC, Zhao TB, Tan YL et al (2015) Reconstruction and numerical test of the mesoscopic model of rock based on Otsu digital image processing. *Rock Soil Mech* 36(9):2532–2540 (**In Chinese**)
- Zhang GC, Liang SJ, Tan YL et al (2018) Numerical modeling for longwall pillar design: a case study from a typical longwall panel in China. *J Geophys Eng* 15(1):121–134
- Zhao TB, Yin YC, Tan YL et al (2014) Bursting liability of coal research of heterogeneous coal based on particle flow microscopic test. *J China Coal Soc* 39(2):280–285 (**In Chinese**)
- Zhao TB, Guo WY, Lu CP et al (2016) Failure characteristics of combined coal–rock with different interfacial angles. *Geomech Eng* 11(3):345–359
- Zhao TB, Guo WY, Tan YL et al (2017) Case histories of rock bursts under complicated geological conditions. *Bull Eng Geol Environ*. <https://doi.org/10.1007/s10064-017-1014-7>
- Zhao TB, Guo WY, Tan YL et al (2018) Case studies of rock bursts under complicated geological conditions during multi-seam mining at a depth of 800 m. *Rock Mech Rock Eng*. <https://doi.org/10.1007/s00603-018-1411-7>
- Zuo JP, Wang ZF, Zhou HW et al (2013) Failure behavior of a rock–coal–rock combined body with a weak coal inter-layer. *Int J Min Sci Technol* 23(6):907–912